Toward a search for axionlike particles at the LNLS

L. Angel,[1,2,*] P. Arias,[3,†] C. O. Dib,[4,‡] A. S. de Jesus,[1,2,§] S. Kuleshov,[5,6,‖] V. Kozhuharov,[7,¶] L. Lin,[8,**] M. Lindner,[9,††] F. S. Queiroz,[1,2,6,‡‡] R. C. Silva,[1,2,§§] and Y. Villamizar[10,‖‖]

[1]*Departamento de Física Teórica e Experimental, Universidade Federal do Rio Grande do Norte, 59078-970, Natal, Rio Grande do Norte, Brazil*
[2]*International Institute of Physics, Universidade Federal do Rio Grande do Norte, Campus Universitário, Lagoa Nova, Natal, Rio Grande do Norte, 59078-970, Brazil*
[3]*Departamento de Física, Universidad de Santiago de Chile, Casilla 307, Santiago, Chile*
[4]*Departamento de Física and CCTVal, Universidad Técnica Federico Santa María, Valparaíso 2340000, Valparaíso, Chile*
[5]*Center for Theoretical and Experimental Particle Physics, Facultad de Ciencias Exactas, Universidad Andres Bello, Fernandez Concha 700, Santiago, Chile*
[6]*Millennium Institute for Subatomic Physics at High-Energy Frontier (SAPHIR), Fernandez Concha 700, Santiago, Chile*
[7]*Faculty of Physics, Sofia University, 5J. Bourchier Blvd., 1164, Sofia, Bulgaria*
[8]*Laboratório Nacional de Luz Síncrotron—LNLS, Caixa Postal 6192, CEP 13084-971, Campinas, São Paulo, Brazil*
[9]*Max Planck Institut fur Kernphysik, Saupfercheckweg 1, 69117 Heidelberg, Germany*
[10]*Centro de Ciências Naturais e Humanas, Universidade Federal do ABC, 09210-580, Santo André, São Paulo, Brazil*

(Received 7 June 2023; accepted 2 September 2023; published 26 September 2023)

Axionlike particles (ALPs) appear in several dark sector studies. They have gained increasing attention from the theoretical and experimental community. In this work, we propose the first search for ALPs to be conducted at the Brazilian Synchrotron Light Laboratory (LNLS). In this work, we derive the projected sensitivity of a proposed experiment for the production of ALPs via the channel $e^+e^- \to a\gamma$. We show that such an experiment could probe ALP masses between 1–55 MeV, and ALP-electron couplings down to $g_{aee} = 2\text{–}6 \times 10^{-4}$ GeV^{-1} depending on the energy beam, thickness of the target, and background assumptions. Therefore, this quest would cover an unexplored region of parameter space for experiments of this kind, constitute a promising probe for dark sectors, and potentially become the first Latin-American dark sector detector.

DOI: 10.1103/PhysRevD.108.055030

I. INTRODUCTION

The Standard Model (SM) of particle physics has successfully described numerous observed phenomena in nature. However, there remain some missing pieces to the puzzle. One common extension to the SM is the inclusion of new neutral bosons, such as vector, scalar, and pseudoscalar particles. Among the pseudoscalar extensions, the axion is one of the most well-known, having been first introduced in the literature in 1977 [1,2] as a solution to the strong-*CP* problem in QCD. By introducing a new global symmetry, the Peccei-Quinn symmetry, which is spontaneously broken at some high-energy scale and explicitly broken due to instanton effects, the mechanism can resolve the strong-*CP* problem and predict the existence of a new particle, the axion. Alongside axions, new pseudoscalar particles, known as axionlike particles (ALPs), have also emerged as possible extensions to the SM.

*lucia.correa.717@ufrn.edu.br
†paola.arias.r@usach.cl
‡claudio.dib@usm.cl
§alvarosdj@ufrn.edu.br
‖sergey.kuleshov@unab.cl
¶venelin@phys.uni-sofia.bg
**liu@lnls.br
††lindner@mpi-hd.mpg.de
‡‡farinaldo.queiroz@ufrn.br
§§ricardo.rego.115@ufrn.edu.br
‖‖yoxarasv@sprace.org.br

Analogously to axions, ALPs have an effective coupling to photons and possibly to fermions. However, for ALPs, their coupling constant and mass are independent parameters. Their popularity arises from several aspects; if they are light enough, they can be produced nonthermally in the early Universe (e.g., via the misalignment mechanism proposed by Dine and Fischler in 1982 [3]), without the need for messenger particles, and potentially account for the entire dark matter content observed today within a wide parameter space [4–6]. Slim ALPs in a higher mass range, with masses below or around MeV, have been extensively sought after at the intensity frontier [7].

In the intermediate mass range, from MeV up to a few GeV, ALPs have received increasing attention. Their potential to alleviate the tension observed in measuring the anomalous electron and muon magnetic moments [8–10] and as messengers between the SM and invisible (dark matter) sectors [11,12] have been recognized. Constraints on this mass range are mainly provided by colliders, such as *BABAR* [13], CLEO [14], LEP [15], LHC, and CLIC [8], as well as beam dump experiments.

So far, the most studied coupling for ALPs is the one with two photons, which is highly constrained. However, the coupling to fermions still presents an important gap, especially for coupling constants $g_{aee} \lesssim 10^{-2}$ GeV^{-1}, for masses in the GeV range. Supernovae are potential sources of ALPs, and they provide strong constraints on several couplings and mass ranges [16–20]. ALPs in the MeV mass range that feature a coupling to photons are mainly produced through the Primakoff effect, and they later decay, producing a gamma-ray flux that sets the upper bound $g_{a\gamma\gamma} < 10^{-11}$ GeV^{-1} for a mass $m_a \sim 10$ MeV [21,22].

However, if ALPs couple to electrons, they can be produced in the core of a supernova mainly through electron Bremsstrahlung, or if their mass is greater than 10 MeV, through electron-positron annihilation. For sufficiently weak couplings, the ALPs can escape the supernova and decay on their way to Earth. This production mechanism can constrain the parameter space to $g_{aee} > 3 \times 10^{-10}$ GeV^{-1} for $m_a \sim 120$ MeV [23,24]. Despite these severe restrictions, it is important to check the aforementioned parameter space with laboratory experiments that have controlled sources and backgrounds, as the astrophysical environments are not fully modeled in some cases, with significant improvements currently underway [25].

In this study, our objective is to develop a theoretical proposal for an ALP search and evaluate the new physics reach of Search for Dark Sector (SeDS), a detector for the dark matter sector [26] at the UVX Synchrotron. UVX is a second-generation storage ring and synchrotron light source that accelerated electrons to 1.37 GeV [27–29], but it has recently been decommissioned. UVX has been succeeded by Sirius, a fourth-generation storage ring [30–32]. Certain subsystems of UVX may be reutilized to develop a new 1–3 GeV positron accelerator, which would give rise to SeDS, a small-scale fixed target experiment aimed at searching for dark sectors, including ALPs. The design of the proposed detector is illustrated in Fig. 1.

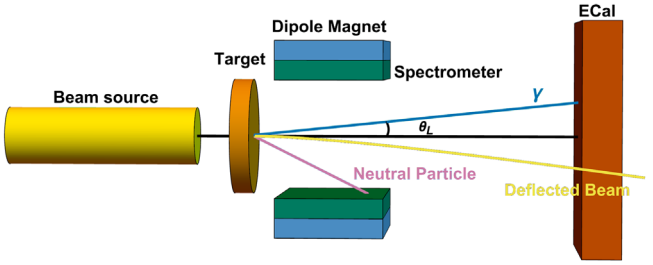

FIG. 1. Experimental scheme of the SeDS experiment. In this scheme, we show the main parts of the experiment, such as the beam source in yellow, the diamond target in orange, the dipole magnet in blue, the spectrometer in green, and the electromagnetic calorimeter in vermilion.

The production process will occur through electron-positron annihilation processes, specifically via channels of the type $e^+e^- \to a\gamma$ as illustrated in Fig. 2. The SeDS experiment will feature a positron beam consisting of 10 bunches of 10^9 positrons on target (POT) per second, with energies ranging from 1 GeV to 3 GeV directed at a diamond target with a thickness of $d = 100$–500 μm. It is well-known that with such an intense beam, a portion of the beam will pass through the target. To address this issue, a magnetic dipole will be added to sweep the noninteracting positron beam away from the calorimeters. This dipole magnet will function as a filter, reducing the number of events in the electromagnetic calorimeter (ECal). Furthermore, a spectrometer is expected to be installed between the gap in the dipole magnet to detect possible positrons that would radiate bremsstrahlung photons, suppressing this background source. On the other hand, since the photons are not affected by the magnetic dipole, they will hit the calorimeter, be measured, and be used to reconstruct the ALP mass using the missing-mass

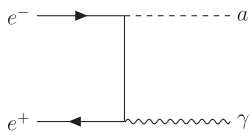

(a) Electron mediated channel.

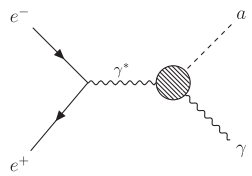

(b) Photon mediated channel.

FIG. 2. Feynman diagrams of the channels that contribute to the ALP production via electron-positron annihilation into a photon and the ALP ($e^+e^- \to a\gamma$).

technique. This setup is expected to yield accurate and precise measurements of the ALP mass. We will show that SeDS has the potential to significantly contribute to the search for ALPs and deepen our understanding of the possible dark sectors.

The missing-mass technique is based on 4-momentum conservation, depending only on the initial parameters of the setup and knowledge about the outgoing photon 4-momentum. With the missing-mass technique the mass of the ALP is given by

$$M^2_{\text{miss}} = (p_{e^-} + p_{\text{beam}} - p_\gamma)^2, \tag{1}$$

where p_{e^-}, p_{beam} and p_γ are the 4-momentum of the target's electrons, positron beam, and outgoing photon, respectively.

The rest of this article is organized as follows. In Sec. II we describe the model for the ALP we consider. In Sec. III we analyze and discuss the observability and bounds of the ALP. Section IV contains our conclusions.

II. THE MODEL

As our model, we consider a straightforward case of ALPs that interact only with photons and electrons,[1] resulting in the following Lagrangian,

$$\mathcal{L} \supset \frac{1}{2}(\partial_\mu a)(\partial^\mu a) - \frac{1}{2}m_a a^2 + \frac{1}{4}g_{a\gamma\gamma} a F_{\mu\nu}\tilde{F}^{\mu\nu} + \frac{g_{aee}}{2}(\partial_\mu a)(\bar{e}\gamma^\mu\gamma^5 e), \tag{2}$$

where $F_{\mu\nu}$ is the electromagnetic strength tensor, $\tilde{F}^{\mu\nu} = \frac{1}{2}\epsilon^{\mu\nu\alpha\beta}F_{\alpha\beta}$ is the dual tensor, m_a is the ALP mass, $g_{a\gamma\gamma}$ is the effective coupling of the ALPs with the photon and g_{aee} being the effective coupling of the axial interaction of the ALPs with the electron, both with dimension of inverse energy.

Since the ALP only interacts with photons and electrons, it has two main decay channels, $a \to \gamma\gamma$ and $a \to e^+e^-$. The decay widths of these channels are given by

$$\Gamma_{a\to\gamma\gamma} = \frac{g^2_{a\gamma\gamma}m_a^3}{64\pi}, \tag{3}$$

$$\Gamma_{a\to e^+e^-} = \frac{g^2_{aee}}{8\pi}m_e^2 m_a\sqrt{1-\frac{4m_e^2}{m_a^2}}. \tag{4}$$

We remind the reader that our proposal is based on the search for ALPs via the process $e^+e^- \to a\gamma$. There are two different channels that can produce ALPs with this signature, represented by the diagrams in Fig. 2. The total cross-section of these channels are given by $\sigma_T = \sigma_{a\gamma} + \sigma_{ae} + \sigma_{\text{int}}$, with

$$\sigma_{a\gamma} = \alpha_{em}g^2_{a\gamma\gamma}\frac{(s+2m_e^2)(s-m_a^2)^3}{24\beta s^4}, \tag{5}$$

$$\sigma_{ae} = \alpha_{em}g^2_{aee}m_e^2\frac{-2m_a^2\beta s + (s^2+m_a^4-4m_a^2m_e^2)\log\frac{1+\beta}{1-\beta}}{2(s-m_a^2)s^2\beta^2}, \tag{6}$$

$$\sigma_{\text{int}} = \alpha_{em}g_{a\gamma\gamma}g_{aee}m_e^2\frac{(s-m_a^2)^2}{2\beta^2 s^3}\log\frac{1+\beta}{1-\beta}, \tag{7}$$

where $\sqrt{s} = \sqrt{2m_e(m_e + E_{\text{beam}})}$ is the center-of-mass (c.m.) energy, m_e is the electron mass, $\beta = \sqrt{1-4m_e^2/s}$ and $\alpha_{em} = e^2/4\pi$ is the electromagnetic fine structure constant. The first equation ($\sigma_{a\gamma}$) is the contribution from the diagram in Fig. 2(a), representing the cross section of the photon-mediated channel as a function of m_a, whilst the second equation (σ_{ae}) is for the diagram in Fig. 2(b). The last equation is the interference term between the two contributions.

It is important to note that ALPs can be produced through other channels, such as Bremsstrahlung with the target ($e^+ + N \to e^+ + N + a$) and Primakoff production originating from a secondary photon that collides with the target ($\gamma + N \to N + a$). However, these channels produce a distinct signal from the previously discussed ones, and the missing mass technique described in Eq. (1) cannot be employed in the same manner since there are no photons in the final state. Hence, these channels do not represent a feasible signal for our setup. An important ingredient of dark sector searches is the decay length. One needs to know whether the ALP will decay inside or outside the detector.

A. Decay length

The first method presented in this work is the so-called invisible search, which is concentrated on the visible counterpart of the signal, i.e., the recoil photon in the final state. However, depending on the detector setup and properties of the ALP, the decay products of the ALP can also be measured, if it decays inside the detector. The latter is known as visible search. A key quantity in this case is the decay length, which is found to be

$$L_a = \gamma\beta c\tau_a \approx \frac{E_a}{m_a\Gamma_a}, \tag{8}$$

where $\gamma = E_a/m_a$ is the Lorentz factor, $\tau_a = \Gamma_a^{-1}$ is the lifetime of the ALP, which is inversely related to the decay width presented in Eq. (4), $\beta = \sqrt{1-4m_e^2/s}$, and E_a being the energy of the ALP. In order to determine the decay length of the ALP to assess whether it decays inside or

[1]Actually, even if we remove the photon interaction at tree level, a similar term would be induced at loop level [8].

outside the detector, we need to know the energy of the ALP, E_a. The energy of the ALP is related to the outgoing photon energy,

$$E_a = \frac{s}{2m_e} - E_{\gamma L}, \tag{9}$$

where $E_{\gamma L}$ is the energy of the photon in the laboratory system, which depends on the opening angle of the photon in relation to the beam axis, and the mass of the ALP as follows:

$$E_{\gamma L} = \left(1 - \frac{m_a^2}{s}\right) m_e \frac{1 + \beta \cos^2\theta_L \sqrt{1 + \tan^2\theta_L}}{1 - \beta^2 \cos^2\theta_L}, \tag{10}$$

where β is the velocity of the c.m. in the laboratory frame and θ_L is the angle between the photon and the beam axis.

In order to clearly demonstrate how the energy and angle of the photon detected in the calorimeter are influenced by the ALP mass, we present the results from Eq. (10) for two different beam energies in Fig. 3 from where it can be inferred that the energy of the outgoing photon increases as the opening angle decreases. Furthermore, in order to accurately determine the mass of the ALP produced in the collision, it is crucial to use a calorimeter with a good energy resolution, especially for photons detected at a high opening angle.

The energy measurement of an electromagnetic calorimeter is determined by the energy released in the detector material through ionization and excitation processes, which is proportional to the energy of the incident particle. The thickness of the absorber layers in radiation lengths affects the energy resolution of an electromagnetic calorimeter, with a smaller thickness leading to a larger number of detected particles and a better energy resolution [33]. To achieve precise determination of the photon energy and ALP mass, it is important to reduce the thickness of the absorber layers. A bismuth-germanate (BGO) calorimeter has achieved an energy resolution of $2\%/\sqrt{E(\mathrm{GeV})}$ [34,35], which is sufficient for our scientific goal. For example, a 100 MeV photon would yield a 6% energy resolution. With a lutetium-yttrium-orthosilicate (LYSO) calorimeter one could improve this energy resolution by a factor of two [36–38].

Having that in mind, we use the measured $E_{\gamma L}$, combined with knowledge of the beam energy to derive E_a, and subsequently determine the decay length of the ALP using Eq. (8) for $E_{\mathrm{beam}} = 1$ GeV [Fig. 4(a)] and $E_{\mathrm{beam}} = 3$ GeV (Fig. 4b). In Fig. 4, we present the decay length of the ALP as a function of the photon angle in the laboratory frame θ_L, assuming a coupling of the ALP with the electron of $g_{aee} = 10^{-3}$ GeV^{-1}, and various values of m_a within the region of interest. Notably, for this configuration, the decay length of the ALP is greater than 20 meters, resulting in the ALP being invisible. However, this is not true when assuming larger couplings, where the decay length of the ALP is orders of magnitude smaller. Nonetheless, the experimental setup is also able to detect ALPs visibly when assuming larger couplings by realizing an inclusive reconstruction with the calorimeter and spectrometer. Therefore, our proposal is to search for ALPs both visibly and invisibly, with the main focus of this work being the invisible channel. Having established the search for ALPs we will address the production cross section.

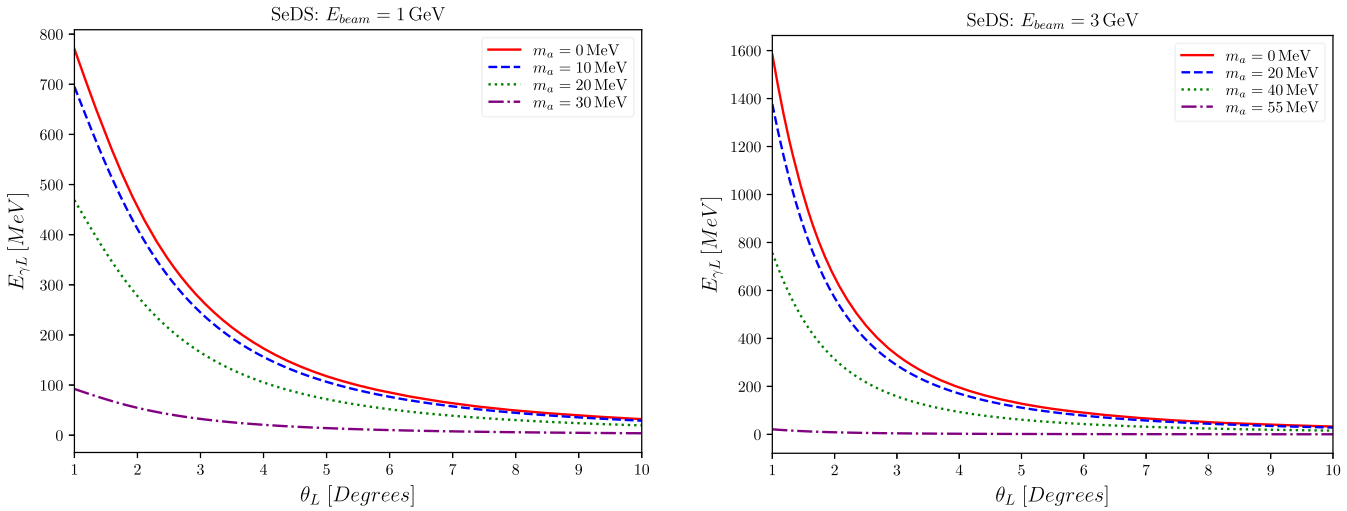

(a) Photon energy for $E_{beam} = 1\,\mathrm{GeV}$. (b) Photon energy for $E_{beam} = 3\,\mathrm{GeV}$.

FIG. 3. Energy of the photon produced along with the ALP as a function of the opening angle between the photon and the beam axis in the laboratory frame for different configurations of the ALP mass. As expected, the photon's energy gets smaller as larger masses are assumed.

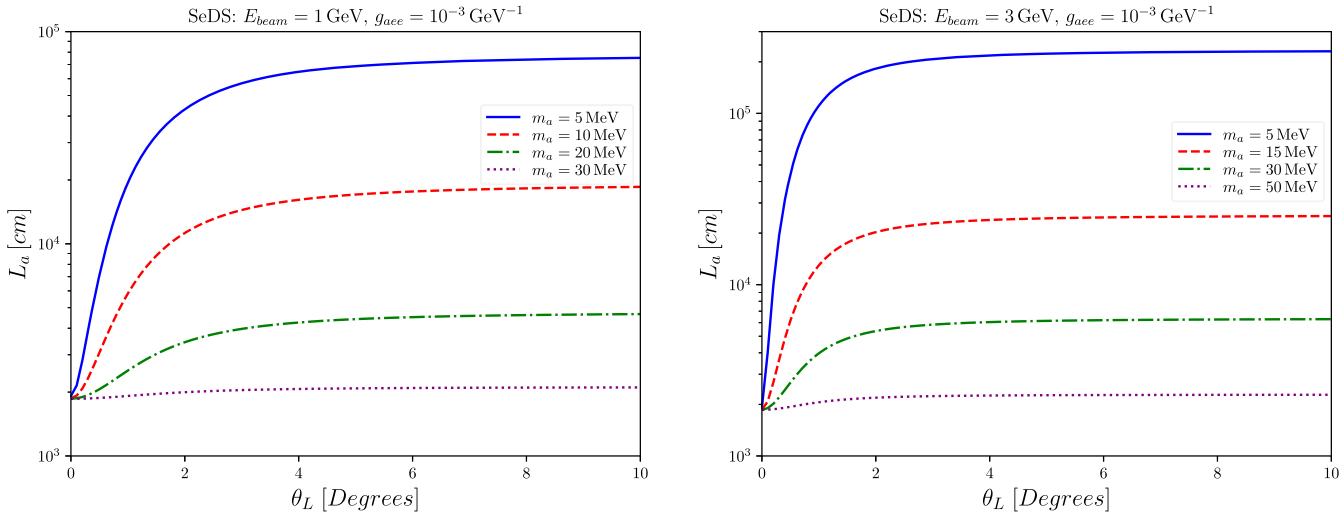

(a) Decay length for $E_{beam} = 1\,\mathrm{GeV}$. (b) Decay length for $E_{beam} = 3\,\mathrm{GeV}$.

FIG. 4. Decay length of the ALP as a function of the photon angle θ_L in the laboratory frame, taking $g_{aee} = 10^{-3}$ for $E_{\mathrm{beam}} = 1$ GeV [Fig. 4(a)] and $E_{\mathrm{beam}} = 3$ GeV [Fig. 4(b)]. Notably, the ALP will decay outside the detector.

III. DISCUSSION

Upon analyzing the total cross section, it has been observed that the interference term is suppressed by a factor of m_e^2. As a result, the contribution of the interference term to the total cross-section is at most 3.5% compared to the case where no interference is present. Thus, we will ignore it and focus on investigating the two ALPs production cross sections, namely $\sigma_{a\gamma}$ and σ_{ae}, independently.

The contributions of the photon and electron mediated channels can be seen in Fig. 5, where we plotted $\sigma_{a\gamma}$ and σ_{ae} for the beam energies of $E_{\mathrm{beam}} = 1$ GeV and $E_{\mathrm{beam}} = 3$ GeV. The contribution of the photon (electron) channel is presented in solid (dashed) lines. We assumed $g_{a\gamma\gamma} = g_{aee} = 1\ \mathrm{GeV}^{-1}$. Although we acknowledge that $g_{a\gamma\gamma} = 1\ \mathrm{GeV}^{-1}$ is excluded by observations, we aim to emphasize the significance of $g_{a\gamma\gamma}$ in the production of ALPs via e^+e^- annihilations. Furthermore, when $m_a \simeq \sqrt{s}$, we find a divergence at σ_{ae}, as shown in the denominator of Eq. (6).

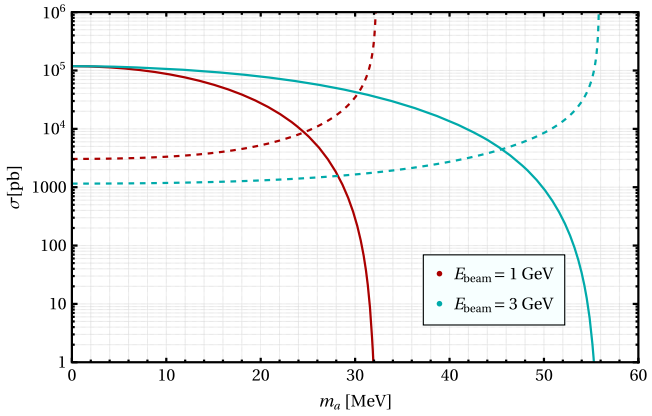

FIG. 5. Cross section of the photon (solid lines) and electron (dashed lines) mediated processes of ALP production as a function of the ALP mass m_a. We considered $g_{a\gamma\gamma} = g_{aee} = 1\ \mathrm{GeV}^{-1}$ and beam energies of 1 GeV and 3 GeV. The drop (peak) in the photon (electron) cross section occurs due to the dependence on m_a, happening for $m_a = 32$ MeV and $m_a = 55$ MeV for the 1 GeV and 3 GeV beams, respectively.

When the couplings have comparable magnitudes, the photon-mediated process's contribution dominates most of the parameter space. However, as the mass of the ALP approaches the center of mass energy, the electron-mediated process becomes the dominant channel. The center-of-mass energy is determined by $\sqrt{s} = \sqrt{2E_{\mathrm{beam}}m_e}$ and is equal to 31.9 MeV and 55.3 MeV for beam energies of 1 GeV and 3 GeV, respectively. Hence, when $g_{a\gamma\gamma} \ll g_{aee}$ the ALP production is governed by g_{aee}. Having in mind the restrictive bounds on $g_{a\gamma\gamma}$, we will assume that g_{aee} is sufficiently larger than $g_{a\gamma\gamma}$, hereafter. That said, we will concentrate our work on g_{aee} in what follows.

A. Current and projected bounds on the model

There are several limits on ALPs stemming from beam dump experiments [39–41], cosmology [42], and astrophysical sources [24,43], which is the main source of these constraints. However, probing such interactions in accelerators would be desirable as it would be subject to smaller systematic uncertainties. In this study, we will focus on the couplings between ALPs and electrons, specifically g_{aee}, which can be directly probed using e^+e^- collisions. To assess the relevance of our proposal, we will put our findings into perspective with existing and projected

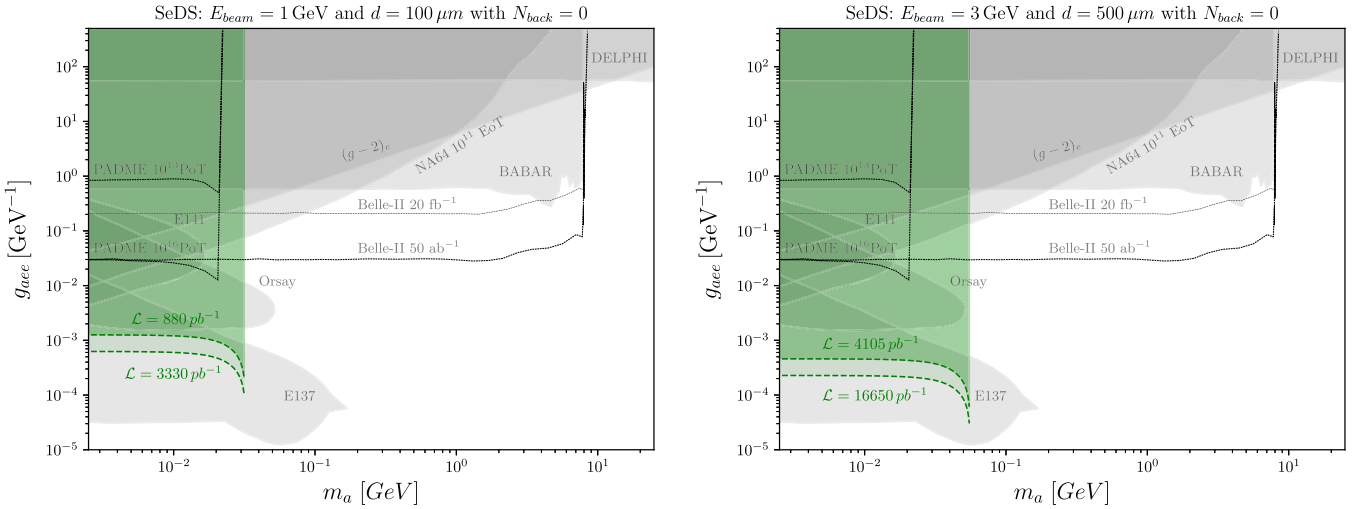

(a) Sensitivity for $E_{beam} = 1\,\mathrm{GeV}$. (b) Sensitivity for $E_{beam} = 3\,\mathrm{GeV}$.

FIG. 6. Current and projected bounds for the g_{aee} coupling in ALP searches for the case where $g_{a\gamma\gamma} = 0$. SeDS' projected sensitivity for $N_{\mathrm{back}} \sim 0$ is presented in the green region. Current and projected limits considered here were taken from [10,40,52,53], where the dashed black lines represent the projected bounds from Belle-II and PADME, while the gray regions are bounds from current and old experiments as well as the ALP contribution to the anomalous magnetic moment of the electron.

accelerator searches. We will outline the relevant bounds on this coupling below:

(i) *DELPHI-LEP*: The DELPHI experiment was a detector inside the Large Electron Positron (LEP) collider at CERN [44]. A revision of the data from the DELPHI experiment on monophoton processes of the type $e^+e^- \to X\gamma$ resulted in $g_{aee} < 8 \times 10\ \mathrm{GeV}^{-1}$ [45]. The excluded region is shown in Figs. 6–8.

(ii) *BABAR*: *BABAR* is a e^+e^- collider [46]. The *BABAR* Collaboration analyzed the production of dark photon in the process $e^+e^- \to A'\gamma$ where A' represents the dark photon, decaying into $e^+e^-, \mu^+\mu^-$ [47]. Recasting this bound, we find $g_{aee} < 0.6\ \mathrm{GeV}^{-1}$ for $1\ \mathrm{MeV} < m_a < 10\ \mathrm{GeV}$. This constraint is exhibited in Figs. 6–8.

(iii) *Belle-II*: The Belle-II experiment [48] has a similar setup to *BABAR*, being able to search for visible

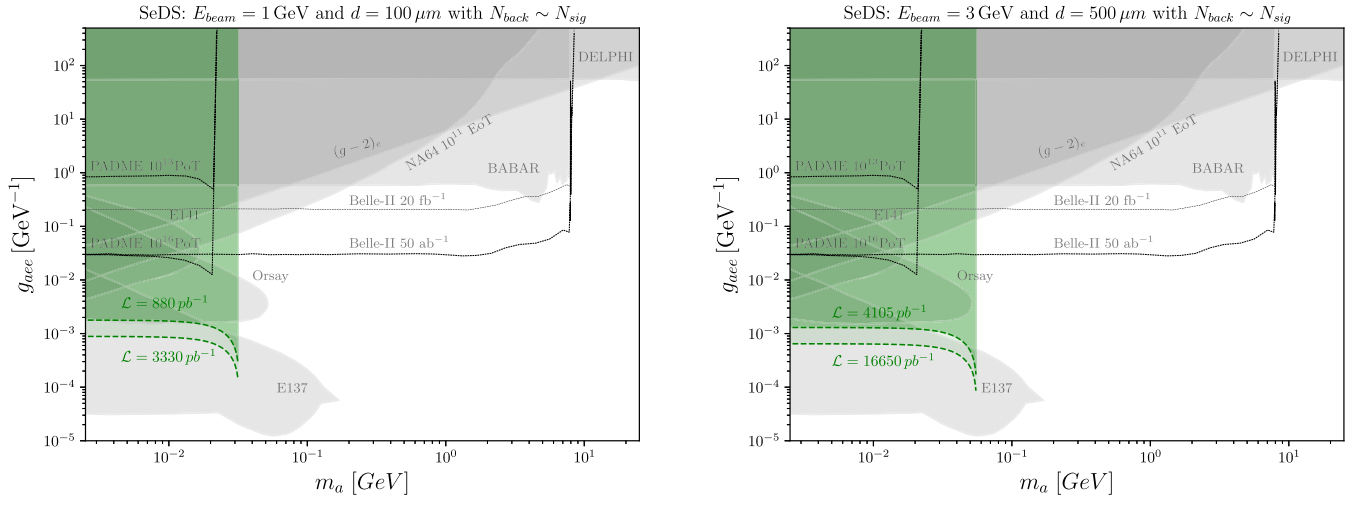

(a) Sensitivity for $E_{beam} = 1\,\mathrm{GeV}$. (b) Sensitivity for $E_{beam} = 3\,\mathrm{GeV}$.

FIG. 7. Current and projected bounds for the g_{aee} coupling in ALP searches for the case where $g_{a\gamma\gamma} = 0$. SeDS' sensitivity for $N_{\mathrm{back}} \sim N_{\mathrm{sig}}$ is presented in the green region. Current and projected limits considered here were taken from [10,40,52,54], where the dashed black lines represent the projected bounds from Belle-II and PADME, while the gray regions are bounds from current and old experiments as well as the ALP contribution to the anomalous magnetic moment of the electron.

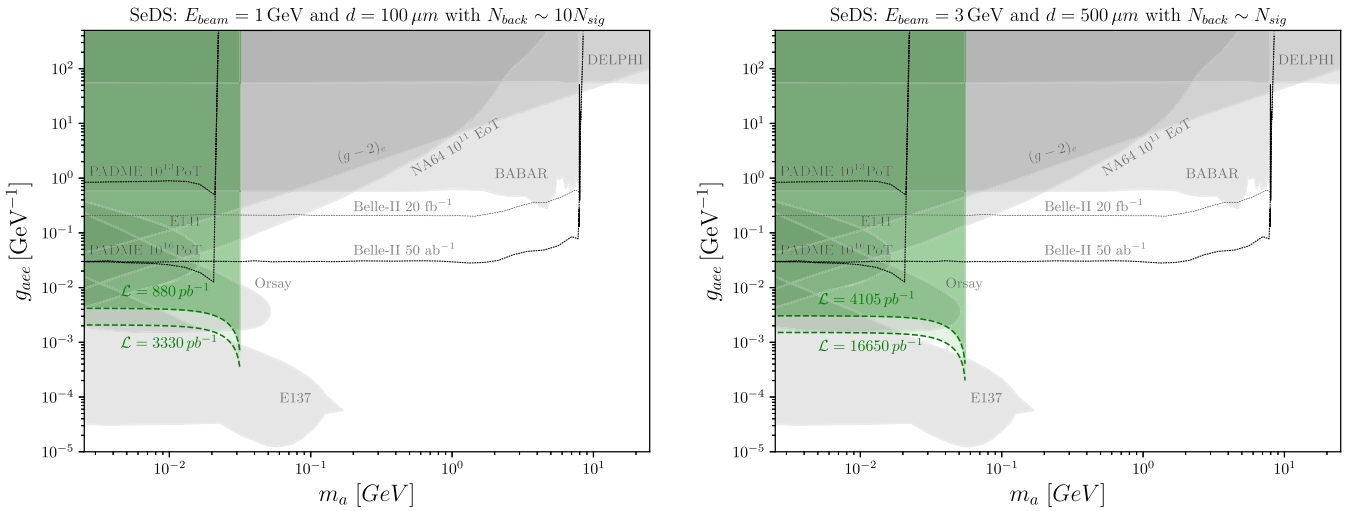

(a) Sensitivity for $E_{beam} = 1\,\mathrm{GeV}$. (b) Sensitivity for $E_{beam} = 3\,\mathrm{GeV}$.

FIG. 8. Same as Figs. 6 and 7, but with $N_{\mathrm{back}} \sim 10 N_{\mathrm{signal}}$.

and invisible ALPs. The projected bounds coming from Belle-II are initially on $g_{a\gamma\gamma}$, but they can be translated to g_{aee}. In this work, we considered the Belle-II projections for the luminosity of 20 fb^{-1} and 50 ab^{-1}. This high luminosity makes this projection produce the most compelling constraints covering most regions of parameter space, being the best probe for ALPs in the range of hundreds of MeV to 10 GeV. The projection for both luminosity configurations is given in Figs. 6–8.

(iv) *NA64*: The NA64 experiment [49] consists of a beam of electrons with an energy of 100 GeV dumped at a fixed target. The experiment goal is to search for dark photons via the process $e^- + Z \to e^- + Z + A'$, where A' is the dark photon that can decay visibly and invisibly, being able to analyze data from the decays $A' \to e^+e^-, \gamma\gamma$. The results of NA64 were used to search for ALPs [39]. As no excess of events was observed, a bound was derived on the ALP-electron couplings, as shown in Figs. 6–8.

(v) *PADME*: The PADME experiment at the DAΦNE Linac features a positron beam with variable energy of 200–550 MeV directed at an active target. Measuring the energy of the final states, the presence of invisible particles such as ALPs can be constrained [50]. During two dedicated runs, the total collected integrated luminosity was $\sim 10^{13}$ POT, with data analysis still in progress. The collaboration also studies the possibility for a new run exploiting the DAΦNE storage ring, for a total of 4×10^{16} POT [10]. The projected bounds are presented in Figs. 6–8.

(vi) *Electron's* $g-2$: The ALP model considered in this work can contribute to the magnetic moment of the electron at the 1-loop level. Thus, the experimental bounds on the anomalous magnetic moment of the electron [51] can be recast as a bound on the parameter space of the model, as presented in Figs. 6–8.

(vii) *Beam dumps*: Data from past beam dump such as the E137, E141, and Orsay experiments [40,52,53] can also be used to generate bounds on the parameter space of visibly decaying ALPs, constraining a considerable region of parameter space, especially in the lower mass range of $m_a \sim 1$–$200\,\mathcal{O}(\mathrm{MeV})$. These bounds are presented in Figs. 6–8.

Depending on the theoretical assumptions, there are other bounds that can be applied to the model, such as indirect bounds on ALP production via flavor-changing meson decays and weak gauge bosons contributions from chiral anomalies as shown in [55]. However, we will not present those indirect bounds in this work.

B. SM background processes

Standard model processes can generate a signal that resembles $e^+e^- \to a\gamma$. However, it is crucial to note that in the framework we are considering, the ALP has a long decay length and therefore decays outside the detector, resulting in signal events characterized by a single photon in the electromagnetic calorimeter. By using the energy of the beam, we can calculate the ALP mass using Eq. (1).

We used CalcHEP and Geant4 to compute the SM background processes [56–58]. The latter is more important in the presence of bremsstrahlung. The primary background processes arise from $\sigma(e^+e^- \to \gamma\gamma) = 0.93$ mb, $\sigma(e^+Z \to e^+\gamma Z) = 2.2 \times 10^3$ mb, $\sigma(e^+e^- \to e^+e^-\gamma) = 77$ mb, and $\sigma(e^+e^- \to \gamma\gamma\gamma) = 0.02$ mb for a positron beam energy of 1 GeV. Among them, the largest cross section originates from photon bremsstrahlung. However, this background can be effectively reduced

because the photon from bremsstrahlung is almost collinear with the beam and the charged particle will be guided to the spectrometer via the electric dipole. Besides, a positron-electron veto system could also be installed to further control this background [59].

Similarly, the background arising from $e^+e^-\gamma$ production can be managed. Although its cross section is not particularly large, the $\gamma\gamma\gamma$ production presents a challenging background. Due to the phase space, there is a lack of symmetry, which could result in a false signal in the calorimeter, where one high-energy photon is detected, and two low-energy photons would pass undetected. This scenario leads to no significant peak in M^2_{miss}. Consequently, it is challenging to reduce this background by applying cuts on the energy and angular distribution of the calorimeter. Notice that this case is different from the two-photon annihilation production, where there is symmetry in the direction of the photons.

We want to emphasize to the reader that this work is a theoretical proposal for an ALP search using a 3 GeV positron accelerator called SeDS, which is planned to be constructed using parts of a partly decommissioned 1.37 GeV accelerator at the LNLS. Our objective is to estimate the projected sensitivity of such an accelerator without considering detector effects but to demonstrate the physics potential of what could be the first Latin-American dark sector detector. In the following section, we explain how we obtained the projected limits.

C. Limits from SeDS

An important quantity to assess the sensitivity of such an accelerator is the luminosity. The instantaneous luminosity of a positron beam impinging on a target is given by

$$L_{\text{inst}} = \frac{N_{\text{P.O.T}}}{\text{s}} N_A \frac{Z\rho d}{A}, \tag{11}$$

where $N_{\text{P.O.T}}/\text{s} = 10^{10}$ is the number of positrons on the target per second considering the properties of the decommissioned accelerator. Assuming a diamond target with a thickness of $d = 100$–500 μm, we can calculate the instantaneous luminosity knowing that N_A is the Avogadro number, $Z = 6$ is the atomic number of the diamond target, $\rho = 3,\ 51\ \text{g/cm}^3$ is the density of diamond and $A = 12.01$ g is the carbon's gram-molecular weight.

We consider two different setups. One uses a 1 GeV positron beam, and the other uses a 3 GeV positron beam. With $E_{\text{beam}} = 1$ GeV and $d = 100$ μm, we find $\mathcal{L} = 821\ \text{pb}^{-1}$ for 90 days of data taking, and $\mathcal{L} = 3331\ \text{pb}^{-1}$ for one year of data taking. For $E_{\text{beam}} = 3$ GeV and $d = 500$ μm, we find $\mathcal{L} = 4106\ \text{pb}^{-1}$ for 90 days of data taking, and $\mathcal{L} = 16650\ \text{pb}^{-1}$ for one year of data taking.

Knowing the luminosity of the experiment, we can calculate the number of signal events and delimit the region of parameter space in which an ALP could be observed in the $\{m_a, g_{aee}\}$ plane assuming $g_{a\gamma\gamma} = 0$.

In Fig. 6, we present the regions at 95% confidence level (CL) assuming that the number of signal events is dominant over the number of background events ($N_{\text{back}} \sim 0$). In Fig. 7, we consider the number of background events, which includes the irreducible background ($e^+e^- \to \gamma\gamma\gamma$), to be similar to the number of signal events. Lastly, in Fig. 8, we assume the number of background events to be ten times larger than the number of signal events. These figures demonstrate that SeDS is a promising probe for directly measuring ALP couplings to electrons, even in a very conservative scenario. It is important to note that these sensitivity projections do not take into account detector effects, but rather serve to demonstrate the physics potential of SeDS as the first Latin-American dark sector detector. Moreover, we did not account for the decay width factor at the resonance, justifying the sharp peak at $\sqrt{s} = m_a$.

Figure 6(a) accounts the projected sensitivity of SeDS for the case $E_{\text{beam}} = 1$ GeV and $d = 100$ μm. In this setup, SeDS probes ALP-electron coupling down to $g_{aee} \sim 6 \times 10^{-4}\ \text{GeV}^{-1}$ for masses up to $m_a \sim 32$ MeV. Figure 6(b) exhibits the sensitivity for $E_{\text{beam}} = 3$ GeV and $d = 500$ μm. In the latter setup, SeDS could probe ALP-electron coupling down to $g_{aee} \sim 2.3 \times 10^{-4}\ \text{GeV}^{-1}$ covering larger ALP masses up to $m_a \approx 55$ MeV due to the larger center-of-mass energy. It is noteworthy that the higher luminosity and center-of-mass energy of the latter configuration can achieve better results than the first one. In both cases, SeDS presents a promising prospect in the search for an electrophilic axionlike particle and projects better results than other experiments of its kind.

However, it is important to note that the sensitivity presented in Fig. 6 is the result of an optimistic analysis in which the experiment's background can be reduced as much as possible, ensuring that the signal is considerably higher than the background. To present a more realistic scenario of SeDS's sensitivity for the electron-mediated channel, Fig. 7 shows the case where $N_{\text{back}} \sim N_{\text{signal}}$.

The first scenario considered is the setup with $E_{\text{beam}} = 1$ GeV and $d = 100$ μm, presented in Fig. 7(a). In this case, SeDS can probe the ALP-electron coupling for values of $g_{aee} > 9 \times 10^{-4}\ \text{GeV}^{-1}$ with $\mathcal{L} = 3300\ \text{pb}^{-1}$. In the second experimental setup where $E_{\text{beam}} = 3$ GeV and $d = 500$ μm, SeDS can reach an ALP-electron coupling of $g_{aee} > 6.5 \times 10^{-4}\ \text{GeV}^{-1}$. As expected, SeDS's sensitivity is reduced when there is a nonzero background. Nevertheless, SeDS's projected sensitivity is still an improvement compared to the results of similar experiments.

In a similar vein, we consider a very conservative scenario where we repeat the exercise above assuming the number of background events to be ten times larger than the signal

events, $N_{\mathrm{sig}} = 10N_{\mathrm{back}}$, in Figs. 8(a) and 8(b). Even so, SeDS covers an unexplored region of parameter space.

IV. CONCLUSION

In this work, we have proposed the first direct search for axionlike particles at the LNLS using a detector named SeDS, which consists of a 1–3 GeV accelerator impinging on a target planned to be constructed using subsystems of UVX, a 1.37 GeV accelerator which has been recently decommissioned. We have concluded that SeDS could place competitive bounds on the coupling of axionlike particle coupling to electrons. In particular, in a conservative scenario, we have shown that SeDS could surpass current and projected similar experiments in the mass range of 1–30 MeV using a 1 GeV positron beam. In an optimistic configuration with a 3 GeV positron beam, SeDS could potentially probe axionlike particles for masses up to 55 MeV and outperform current and projected experiments of the kind, probing g_{aee} down to 3×10^{-4} GeV^{-1}.

ACKNOWLEDGMENTS

We would like to thank Harry Westfahl, Daniel Tavares, and Narcizo Neto from the LNLS for their hospitality and for providing useful information about the accelerator. *Funding:* Simons Foundation (Award No. 1023171-RC), FAPESP Grants No. 2018/25225-9, No. 2021/01089-1, and No. 2023/01197-4, ICTP-SAIFR FAPESP Grant No. 2021/14335-0, CNPq Grant No. 307130/2021-5, ANID-Programa Milenio-code ICN2019_044, CAPES Grant No. 88887.485509/2020-00, ANID-Programa Milenio-code ICN2019_044, ANID PIA/APOYO AFB180002 (Chile), ANID/CONICYT FONDECYT Regular 1221463 and FONDECYT Regular 1210131. Y. V. expresses gratitude to São Paulo Research Foundation (FAPESP) under Grant No. 2018/25225-9 and 2023/01197-4. In addition, V. K. recognizes that partially this study is financed by the European Union-NextGenerationEU, through the National Recovery and Resilience Plan of the Republic of Bulgaria, Project No. SUMMIT BG-RRP-2.004-0008-C01.

[1] R. D. Peccei and Helen R. Quinn, *CP* Conservation in the Presence of Pseudoparticles, Phys. Rev. Lett. **38**, 1440 (1977).
[2] R. D. Peccei and Helen R. Quinn, Constraints imposed by *CP* conservation in the presence of pseudoparticles, Phys. Rev. D **16**, 1791 (1977).
[3] Michael Dine and Willy Fischler, The not so harmless axion, Phys. Lett. **120B**, 137 (1983).
[4] Eduard Masso and Ramon Toldra, On a light spinless particle coupled to photons, Phys. Rev. D **52**, 1755 (1995).
[5] Paola Arias, Davide Cadamuro, Mark Goodsell, Joerg Jaeckel, Javier Redondo, and Andreas Ringwald, WISPy cold dark matter, J. Cosmol. Astropart. Phys. 06 (2012) 013.
[6] Dilip Kumar Ghosh, Anish Ghoshal, and Sk Jeesun, Axion-like particle (ALP) portal freeze-in dark matter confronting alp search experiments, arXiv:2305.09188.
[7] J. L. Hewett, *Fundamental physics at the intensity frontier. Report of the workshop held December 2011 in Rockville, MD* (2012), 10.2172/1042577.
[8] Martin Bauer, Matthias Neubert, and Andrea Thamm, Collider probes of axion-like particles, J. High Energy Phys. 12 (2017) 044.
[9] Darwin Chang, We-Fu Chang, Chung-Hsien Chou, and Wai-Yee Keung, Large two loop contributions to g-2 from a generic pseudoscalar boson, Phys. Rev. D **63**, 091301 (2001).
[10] Luc Darmé, Federica Giacchino, Enrico Nardi, and Mauro Raggi, Invisible decays of axion-like particles: Constraints and prospects, J. High Energy Phys. 06 (2021) 009.
[11] Marat Freytsis and Zoltan Ligeti, Dark matter models with uniquely spin-dependent detection possibilities, Phys. Rev. D **83**, 115009 (2011).
[12] Keith R. Dienes, Jason Kumar, Brooks Thomas, and David Yaylali, Overcoming velocity suppression in dark-matter direct-detection experiments, Phys. Rev. D **90**, 015012 (2014).
[13] J. P. Lees *et al.*, Search for Invisible Decays of a Dark Photon Produced in e^+e^- Collisions at *BABAR*, Phys. Rev. Lett. **119**, 131804 (2017).
[14] R. Balest *et al.*, $\Upsilon(1S) \to \gamma +$ noninteracting particles, Phys. Rev. D **51**, 2053 (1995).
[15] Joerg Jaeckel and Michael Spannowsky, Probing MeV to 90 GeV axion-like particles with LEP and LHC, Phys. Lett. B **753**, 482 (2016).
[16] Shao-Feng Ge, Koichi Hamaguchi, Koichi Ichimura, Koji Ishidoshiro, Yoshiki Kanazawa, Yasuhiro Kishimoto, Natsumi Nagata, and Jiaming Zheng, Supernova-scope for the direct search of supernova axions, J. Cosmol. Astropart. Phys. 11 (2020) 059.
[17] Jeremy Sakstein, Djuna Croon, and Samuel D. McDermott, Axion instability supernovae, Phys. Rev. D **105**, 095038 (2022).
[18] Kanji Mori, Takashi J. Moriya, Tomoya Takiwaki, Kei Kotake, Shunsaku Horiuchi, and Sergei I. Blinnikov, Light curves and event rates of axion instability supernovae, Astrophys. J. **943**, 12 (2023).
[19] Sebastian Hoof and Lena Schulz, Updated constraints on axion-like particles from temporal information in supernova sn1987a gamma-ray data, J. Cosmol. Astropart. Phys. 03 (2023) 054.

[20] Melissa Diamond, Damiano F. G. Fiorillo, Gustavo Marques-Tavares, and Edoardo Vitagliano, Axion-sourced fireballs from supernovae, Phys. Rev. D **107**, 103029 (2023).
[21] J. Jaeckel, P. C. Malta, and J. Redondo, Decay photons from the axionlike particles burst of type II supernovae, Phys. Rev. D **98**, 055032 (2018).
[22] Francesca Calore, Pierluca Carenza, Maurizio Giannotti, Joerg Jaeckel, Giuseppe Lucente, and Alessandro Mirizzi, Supernova bounds on axionlike particles coupled with nucleons and electrons, Phys. Rev. D **104**, 043016 (2021).
[23] Ricardo Z. Ferreira, M. C. David Marsh, and Eike Müller, Strong supernovae bounds on ALPs from quantum loops, J. Cosmol. Astropart. Phys. 11 (2022) 057.
[24] Giuseppe Lucente and Pierluca Carenza, Supernova bound on axionlike particles coupled with electrons, Phys. Rev. D **104**, 103007 (2021).
[25] Pierluca Carenza, Tobias Fischer, Maurizio Giannotti, Gang Guo, Gabriel Martínez-Pinedo, and Alessandro Mirizzi, Improved axion emissivity from a supernova via nucleon-nucleon bremsstrahlung, J. Cosmol. Astropart. Phys. 10 (2019) 016; 05 (2020) E01.
[26] L. Duarte, L. Lin, M. Lindner, V. Kozhuharov, S. V. Kuleshov, A. S. de Jesus, F. S. Queiroz, Y. Villamizar, and H. Westfahl, Search for Dark Sector by Repurposing the UVX Brazilian Synchrotron, Eur. Phys. J. C **83**, 514 (2023).
[27] L. Lin and C. E. T. Goncalves da Silva, Second order single particle dynamics in quasiisochronous storage rings and its application to the LNLS UVX ring, Nucl. Instrum. Methods Phys. Res., Sect. A **329**, 9 (1993).
[28] Lin Liu, Ruy Farias, Ximenes Resende, and Pedro Tavares, Beam based calibration of the LNLS UVX storage ring BPMs, in *Particle Accelerator Conference (PAC 09)* (2010), p. TH6PFP011.
[29] Sofia Lescano, Eduardo Coelho, José Franco, Patricia Nallin, Gustavo Pinton, and Antonio Rodrigues, UVX control system: An approach with beaglebone black, in *Proceedings of the 11th International Workshop on Personal Computers and Particle Accelerator Controls* (JACoW, Geneva, Switzerland, 2017), p. THPOPRPO03.
[30] Antonio Rodrigues *et al.*, Sirius status update, in *Proceedings of the 10th International Particle Accelerator Conference* (JACoW, Geneva, Switzerland, 2019), p. TUPGW003.
[31] Murilo Alves, Lin Liu, and Fernando de Sá, Simulation of sirius booster commissioning, in *Proceedings of the 10th International Particle Accelerator Conference* (JACoW, Geneva, Switzerland, 2019), p. WEPTS105.
[32] Lin Liu, Murilo Alves, Ana Clara Oliveira, Ximenes Resende, and Fernando de Sá, Sirius commissioning results and operation status, in *Proceedings of the 12th International Particle Accelerator Conference* (JACoW, Geneva, Switzerland, 2021).
[33] C. W. Fabjan and F. Gianotti, Calorimetry for particle physics, Rev. Mod. Phys. **75**, 1243 (2003).
[34] A. Frankenthal *et al.*, Characterization and performance of PADME's Cherenkov-based small-angle calorimeter, Nucl. Instrum. Methods Phys. Res., Sect. A **919**, 89 (2019).
[35] B. Bantes *et al.*, The BGO calorimeter of BGO-OD experiment, J. Phys. Conf. Ser. **587**, 012042 (2015).
[36] D. Anderson, A. Apresyan, A. Bornheim, J. Duarte, C. Pena, A. Ronzhin, M. Spiropulu, J. Trevor, and S. Xie, On timing properties of LYSO-based calorimeters, Nucl. Instrum. Methods Phys. Res., Sect. A **794**, 7 (2015).
[37] A. Bornheim, A. Apresyan, A. Ronzhin, S. Xie, J. Duarte, M. Spiropulu, J. Trevor, D. Anderson, C. Pena, and M. H. Hassanshahi, LYSO based precision timing calorimeters, J. Phys. Conf. Ser. **928**, 012023 (2017).
[38] A. M. E. Saad and F. Kocak, Evaluation of energy resolution by changing angle and position of incident photon in a LYSO calorimeter, Acta Phys. Pol. B **51**, 2097 (2020).
[39] D. Banerjee, J. Bernhard *et al.*, Search for Axionlike and Scalar Particles with the NA64 Experiment, Phys. Rev. Lett. **125**, 081801 (2020).
[40] J. D. Bjorken, S. Ecklund, W. R. Nelson, A. Abashian, C. Church, B. Lu, L. W. Mo, T. A. Nunamaker, and P. Rassmann, Search for neutral metastable penetrating particles produced in the slac beam dump, Phys. Rev. D **38**, 3375 (1988).
[41] E. M. Riordan, M. W. Krasny *et al.*, Search for Short-Lived Axions in an Electron-Beam-Dump Experiment, Phys. Rev. Lett. **59**, 755 (1987).
[42] Diptimoy Ghosh and Divya Sachdeva, Constraints on axion-lepton coupling from big bang nucleosynthesis, J. Cosmol. Astropart. Phys. 10 (2020) 060.
[43] Jae Hyeok Chang, Rouven Essig, and Samuel D. McDermott, Supernova 1987a constraints on sub-GeV dark sectors, millicharged particles, the QCD axion, and an axion-like particle, J. High Energy Phys. 09 (2018) 051.
[44] G. D. Alekseev *et al.*, The DELPHI experiment at LEP, Part. Nucl. Lett. **98**, 5 (2001).
[45] J. Abdallah *et al.*, Search for one large extra dimension with the DELPHI detector at LEP, Eur. Phys. J. C **60**, 17 (2009).
[46] P. F. Harrison, An introduction to the *BABAR* experiment, Nucl. Instrum. Methods Phys. Res., Sect. A **368**, 81 (1995).
[47] J. P. Lees, V. Poireau *et al.*, Search for a Dark Photon in e^+e^- Collisions at *BABAR*, Phys. Rev. Lett. **113**, 201801 (2014).
[48] E. Kou, P. Urquijo *et al.*, The Belle II physics book, Prog. Theor. Exp. Phys. **2019**, 123C01 (2019).
[49] D. Banerjee *et al.*, Search for a Hypothetical 16.7 MeV Gauge Boson and Dark Photons in the NA64 Experiment at CERN, Phys. Rev. Lett. **120**, 231802 (2018).
[50] Mauro Raggi and Venelin Kozhuharov, Proposal to search for a dark photon in positron on target collisions at DAΦNE linac, Adv. High Energy Phys. **2014**, 959802 (2014).
[51] Leo Morel, Zhibin Yao, Pierre Clade, and Saida Guellati-Khelifa, Determination of the fine-structure constant with an accuracy of 81 parts per trillion, Nature (London) **588**, 61 (2020).
[52] E. M. Riordan *et al.*, Search for Short-Lived Axions in an Electron-Beam-Dump Experiment, Phys. Rev. Lett. **59**, 755 (1987).
[53] M. Davier and H. Nguyen Ngoc, An unambiguous search for a light higgs boson, Phys. Lett. B **229**, 150 (1989).

[54] A. Konaka, K. Imai, H. Kobayashi, A. Masaike, K. Miyake, T. Nakamura, N. Nagamine, N. Sasao, A. Enomoto, Y. Fukushima, E. Kikutani, H. Koiso, H. Matsumoto, K. Nakahara, S. Ohsawa, T. Taniguchi, I. Sato, and J. Urakawa, Search for Neutral Particles in Electron-Beam-Dump Experiment, Phys. Rev. Lett. **57**, 659 (1986).

[55] Wolfgang Altmannshofer, Jeff A. Dror, and Stefania Gori, New Opportunities for Detecting Axion-Lepton Interactions, Phys. Rev. Lett. **130**, 241801 (2023).

[56] Alexander Belyaev, Neil D. Christensen, and Alexander Pukhov, CalcHEP 3.4 for collider physics within and beyond the standard model, Comput. Phys. Commun. **184**, 1729 (2013).

[57] C. Zeitnitz and T. A. Gabriel, The Geant—CALOR interface and benchmark calculations of ZEUS test calorimeters, Nucl. Instrum. Methods Phys. Res., Sect. A **349**, 106 (1994).

[58] René Brun, F. Bruyant, Federico Carminati, Simone Giani, M. Maire, A. McPherson, G. Patrick, and L. Urban, Geant Detector Description and Simulation Tool (1994), 10.17181/CERN.MUHF.DMJ1.

[59] Isabella Oceano, The PADME charged particle spectrometer, J. Phys. Conf. Ser. **2374**, 012027 (2022).